Available online at www.sciencedirect.com

SciVerse ScienceDirect

Ceramics International 39 (2013) 2753–2765

CERAMICS INTERNATIONAL

www.elsevier.com/locate/ceramint

Sonosynthesis of nanostructured TiO_2 doped with transition metals having variable bandgap

A.K.P.D. Savio, J. Fletcher, F.C. Robles Hernández*

University of Houston, Department of Mechanical Engineering Technology, College of Technology, 304 Technology Building, Houston, TX 77204-4020, USA

Received 17 August 2012; accepted 11 September 2012
Available online 3 October 2012

Abstract

Here is described a sonosynthesis method to produce nanostructured TiO_2 pure and doped (Al, C, Co, Fe and Rh). The synthesized TiO_2 is amorphous and is transformed to anatase, brookite or rutile by heat treatments at temperatures between 100 and 300 °C. Pure TiO_2 can be partially transformed to brookite between 100 and 300 °C. The band gap in all heat treated samples from 100–600 °C is relatively constant, 3.2 eV, except for those doped with Fe. This effect on the band gap is the results of a bi/tri-crystal (anatase:brookite:rutile) framework. Rhodium is the most effective dopant to narrow the band gap, the opposite effect is observed with C. In single phase frameworks the bandgap can be modified ranges from 2.38 to 4.10 eV depending on the dopant. TiO_2 lattices are rigid enough to promote an outwards diffusion of the dopants to the surface of the particles forming nanostructured precipitates. The precipitates develop a network of quantum-dots with sizes between 5 and 10 nm.
Published by Elsevier Ltd

Keywords: C: Optical properties; Spectroscopy; D. TiO_2; Sono-synthesis

1. Introduction

The three allotropes of titanium dioxide (TiO_2) and their respective crystalline structures are: (i) rutile has a $P4_2/mnm$ symmetry with a tetragonal structure, (ii) anatase is $I4_1/amd$ and is a body centered tetragonal and (iii) brookite is P/cab with an orthorhombic structure. Rutile can be obtained from heat treated anatase under different conditions [1–3]. The TiO_2 is widely used for photo catalysis, solar energy conversion, protective surface coating, ceramics, pigments, biological, catalysis, as a reductor, for photo-corrosion applications, etc. [1,3]. In recent years the sono-synthesis has demonstrated success to produce nanostructured TiO_2 [4–6] and other nanostructured materials [7,8]. Anatase seems to be more attractive than rutile for a wide range of applications that is attributed to its lower band gap [3,9–15]. The band gap in anatase and rutile can be controlled by heat and mechanical treatments having direct effects on catalytic and photo catalytic activities [16–18].

Many efforts have been directed to control the TiO_2 nanostructure; however, several problems still remain unsolved. For instance, annealing significantly affects microstructure, crystalline structure, phase(s) and the grain size of TiO_2 that might influence their catalytic and photo catalytic activity. Anatase and rutile are active in the UV range of the spectrum [1,2]. Band gap modifications are attributed to grain size; however, this does not seem to be the main contributor to band gap, but rather the frameworks among anatase, brookite and rutile [19,20].

In the present work is proposed a methodology for in situ doping of the TiO_2 during sonochemistry along with a heat treatment methodology to control phase transformations and grain growth within single, bi- or tri-crystal frameworks. The identified phases in the investigated samples include anatase, brookite and rutile. In this work is proposed a methodology to synthesize TiO_2 with combinations of the above phases and specific bandgaps. The characterization methods used in this work include X-ray diffraction (XRD), Electron (Transmission

*Correspondence to: University of Houston, College of Engineering Technology, 304 Technology Building, Houston, TX 77204-4020, USA. Tel.: +1 713 743 8231; fax: +1 505 213 7106.
E-mail addresses: fcrobles@uh.edu, fcrobles@central.uh.edu (F.C. Robles Hernández).

0272-8842/$ - see front matter Published by Elsevier Ltd
http://dx.doi.org/10.1016/j.ceramint.2012.09.042

Table 1
Chemical agents used in the present work with their respective purity and vendors.

Name	Formula	Purity (wt%)	Vendor
Titanium isopropoxide	$Ti[OCH(CH_3)_2]_4$	97.00	Sigma Aldrich
Aluminum chloride anhydrous, metals basis	$AlCl_3$	99.99	Sigma Aldrich
Carbon soot	C	99.99	SERES
Cobalt (III) fluoride	CoF_3	99.99	Sigma Aldrich
Iron (III) nitrate anhydrous, trace metal basis	$Fe(NO_3)_3$	99.99	Sigma Aldrich
Rhodium (III) nitrate ~36 wt% rhodium	$Rh(NO_3)_3$	99.99	Sigma Aldrich

and Scanning) Microscopy, UV–vis, Raman spectroscopy, and X-ray Photoelectron spectroscopy (XPS), the results of which are provided and discussed.

2. Experimental

2.1. Synthesis

The chemicals used in the present work are described in Table 1. De-ionized water (30 ml) is added drop wise to 150 ml of titanium isopropoxide ($Ti[OCH(CH_3)_2]_4$) during sonication. The temperature in the sonicator was monitored not to exceed 40 °C. The samples were doped with 0.1 at% of Al, C, Co and Fe. Rh additions were at 0.075 and 0.15 at% and the respective samples are identified as $Rh_{0.075}$ and $Rh_{0.15}$. Most of the results presented herein correspond to $Rh_{0.075}$; however, the band gap and other relevant results are presented for both samples.

The titanium isopropoxide is poured into a flask that was submerged in room temperature water that was stirred thoroughly to keep a temperature of 40 °C through the entire synthesis. The sonication was assisted by a Misonix S-2000 apparatus operated with micro-tip using amplitude of 100%, 20 kHz for 30 min delivering 15 j/s. The resulting colloid was placed on a hot plate at 60 °C for 24 h, the resultant powders are TiO_2 with traces of organic residue. The dried powders have a dry and loose appearance. The organic residue is removed by washing the powders several times with de-ionized water and drained using micropore filter paper connected to a vacuum system via funnel-flask. Following the washing procedure the powders are dried again using the process described above.

2.2. Thermal analysis and heat treatment

Thermal analysis for the heat treated samples was carried out using a workstation consisting of a high-speed–high-resolution National Instruments data acquisition system (cFP 1804, Austin, TX) linked to a personal computer. The cFP 1804 data acquisition system has capabilities of up to 4 interchangeable modules with capacity for 8 thermocouples each and is internet (remotely) controlled. The data collection was set to 10 temperature readings per second. The thermal analysis is conducted to determine the transition temperatures for TiO_2. The transition temperatures were identified using the thermal analysis procedures proposed by Robles Hernandez et. al. [21–25].

The synthesized TiO_2 was heat treated at temperatures from 100 °C to 800 °C in a tube electric resistance furnace in open air atmosphere for 12 h. In all cases the heat treatments were performed in open air atmosphere, except for C doped samples. The C doped samples were heat treated in helium atmosphere at a pressure of 100 Torr, this helps preventing excessive interaction among carbon and oxygen to hinder potential oxidation.

2.3. Characterization

The XRD characterization was conducted on a SIEMENS Diffractometer D5000 equipped with a Cu tube and operated at 40 kV and 30 A with a corresponding $K_\alpha = 0.15406$ nm. The lattice parameters ("*a*" and "*c*") for anatase and rutile phases were determined using the $(101)_A$[1]/$(200)_A$ and $(110)_R$[2]/$(101)_R$ reflections respectively. The Scherrer method was used to determine the grain size [26] using the $(101)_A$ $(101)_R$ reflections and the following equation: $D = k\lambda/\beta_{1/2} \cdot \cos\theta$ where: D is the average diameter of the calculated particles, *"k"* is the shape factor of the average crystallite (0.9), λ is the wavelength ($K\alpha$) in Å, $\beta_{1/2}$ is full width half maximum (FWHM) of the X-ray reflection. The Scherrer method was selected due to its relative high accuracy ($\pm 15\%$) when compared to Transmission Electron Microscopy (TEM) [27].

The scanning electron microscopy (SEM) observations were carried on a FEI XL-30FEG using a 15 kV in secondary electrons mode. The samples were prepared depositing the powders directly on graphite tape and coated with gold. High Resolution Transmission Electron Microscopy (HRTEM) samples were prepared by adding a pinch of powder on to a 3 ml of ethanol. The solution was sonicated for 1 min to form a suspension that was allowed to sediment until the liquid has a clear appearance. At that time 2 drops of the suspension were deposited on a Cu grid (300 mesh). The HRTEM was conducted on a JEOL 200 FX operated at 200 kV.

Raman spectroscopy was conducted on an XploRA™ apparatus, using a green laser (532 nm) on medium

[1]The subscript "A" indicates anatase.
[2]The subscript "R" indicates rutile.

intensity and a shift of 1 cm^{-1}, a spot size is 1 μm and a resolution of 0.5 cm^{-1}. Optical spectroscopy characterization was conducted using a Triax 320 monochromator in transmission mode equipped with a broad spectrum Xenon lamp and a UV-enhanced Si photodetector. The spectral measurements were performed using the diffused reflectance method in a wavelength range between 250 and 500 nm. The band gaps were determined with the Kulbeka-Munk method [28].

The samples for Raman and optical spectroscopy were prepared by adding 0.01 g of each powder in 10 ml of deionized water. The mix was subjected to sonication for 10 min using an intensity of 15 j/s. The suspension was deposited on fuse silica glasses (4 mm in diameter) using a spinning-like approach followed by a drying procedure on a hot plate at 60 °C for 2 h. The process was repeated 5 times to thicken the film and obtain representative values.

The x-ray photoelectron spectroscopy (XPS) was conducted on a Physical Electronics XPS Instrument Model 5700. The XPS was operated via monochromatic Al-K_α X-ray source (1486.6 eV) at 350 W. The analyzed area, collection solid cone and take off angle were set at 800 μm, 5° and 45° respectively. A pass energy of 11.75 eV was used to obtain a resolution of 0.51 eV or better. The XPS was conducted in a vacuum below 5×10^{-9} Torr. The data analysis was conducted on Multipak™ software and the Shirley background subtraction routine had been applied throughout.

3. Results

Fig. 1 shows a representative thermal analysis curve for the pure TiO_2 in the as synthesized conditions. The heating curve was recorded and its first derivative was calculated. The first derivative is used to enhance the transformation temperatures allowing relatively easier and more precise identification of the phase transformations [21–23,29]. The transformation temperatures correspond to anatase, brookite, rutile and water that were confirmed with XRD and Raman. The TiO_2 transformation temperatures occur at: 136.16 °C, 280.81 °C, 463.84 °C and 100.5 °C respectively. An important finding is the relatively lower transformation temperatures observed for each phase that is attributed to the effects of sonication along with the grain size. The heating temperatures for thermal analysis were selected to cover the entire transition (anatase–rutile) temperature range. Previous work led to the synthesis of different combinations of phases among pure anatase and rutile or combinations with brookite [30].

Fig. 2 shows the XRD characterization of the as synthesized and heat treated TiO_2. The XRD results indicate that the as synthesized product is quasi-amorphous and transform to anatase at relatively low temperatures, followed by the partial transformation to brookite that is observed only for the pure TiO_2 sample. The diffraction pattern at 200 °C shows the presence of the following anatase reflections: (110), (112), (200), (105) and (211). Brookite is identified by the reflections: (210), (111) and (020) in the heat treated samples between 300 and 500 °C. The overlap between the anatase and brookite reflections limits a precise grain size determination; therefore, the results are not reported. The above suggest a bi-crystal framework among anatase and brookite in samples heat treated between 200 and 300 °C. From 300 to 500 °C there is a tri-crystal framework. The transformation to rutile is initiated at a temperature above 300 °C and

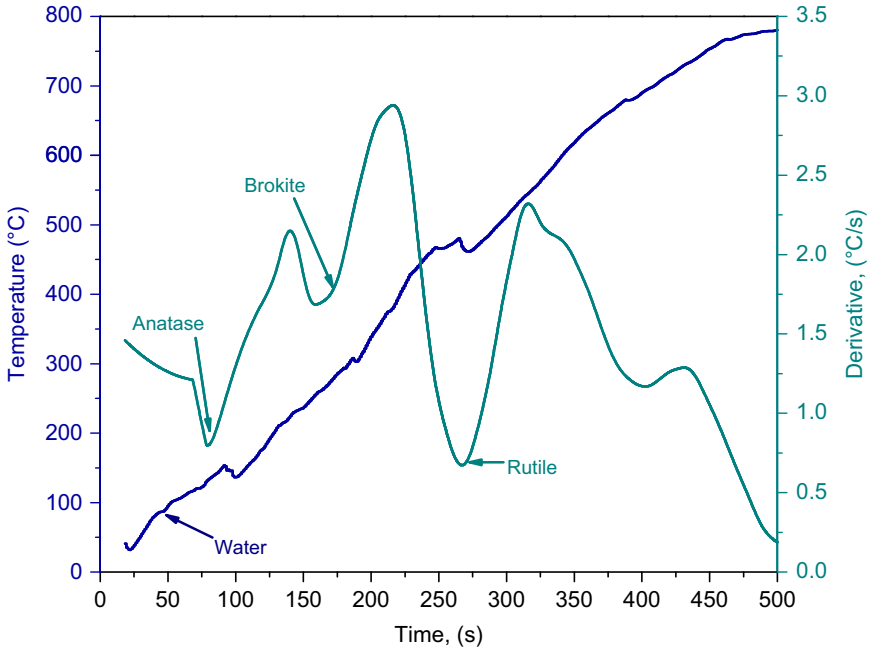

Fig. 1. Thermal analysis results showing the heating and the first derivative curves of the pure TiO_2 sample in the as synthesized conditions heated to approximately 800 °C.

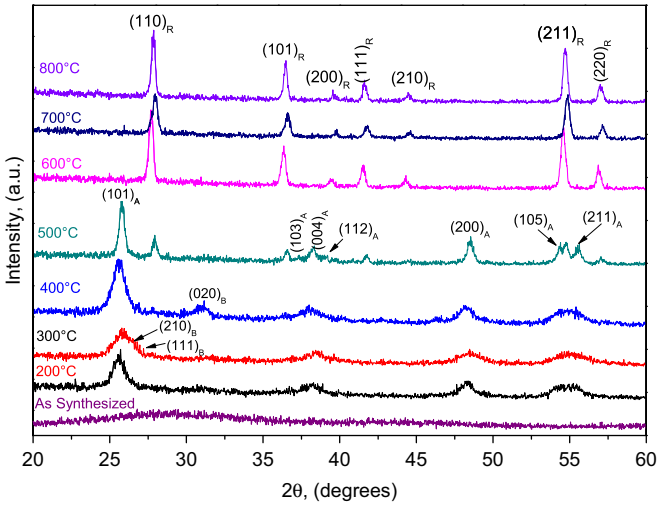

Fig. 2. XRD results of the pure TiO_2 in the as synthesized and heat treated conditions from 200 to 800 °C. The sub scripts (A, B, and R) are used to identify anatase, brookite, and rutile respectively.

completed at around 500 °C. These results are in agreement with the thermal analysis (compare Figs. 1 and 2).

Brookite was not identified in the doped; instead, anatase transform directly to rutile. This transformation occurs at different temperatures and is directly affected by the dopant. The presence of brookite is important since it is a known to be an indirect band gap semiconductor with a narrow band gap (1.9 eV) [31]. It is expected that the complete transformation to brookite can be achieved using pure TiO_2 at the above mentioned temperatures for extended periods of time and is contemplated for our future work.

The XRD and Raman results for the as synthesized and doped TiO_2 samples are given in Fig. 3. The XRD shows a quasi-amorphous phase that is confirmed with Raman for all the samples except for C and Co doped samples. The estimated grain size of the as synthesized TiO_2 is approximately 6.2 nm [1,2,20]. These particles are likely to be composed of TiO_2 with a high density of incomplete bonds. These results are expected and correspond to a quasi-amorphous phase with non-equilibrium stoichiometries that is attributed to a lack of oxygen and hence broken bonds. This is further confirmed by the Raman characterization (Fig. 3b) of the samples doped with Al, Fe and Rh.

The as synthesized C and Co doped samples present intense $E_{g(1)}$ and $E_{g(2)}$ Raman bands respectively. We presume that the high intensity of the $E_{g(1)}$ band in the Co doped sample is well resolved due to a short to mid-range order that is in agreement with the XRD results (Fig. 3a). The local nano-stoichiometry is strongly effecting the C doped characteristics as observed in the Raman results that is due to phonon confinement effects on the $E_{g(1)}$ and $E_{g(2)}$ bands resulting in anomalies related to hydrostatic pressures [32]. We believe that the $E_{g(2)}$ band at 193 cm^{-1} (usually weak [33]) is well resolved and sharp

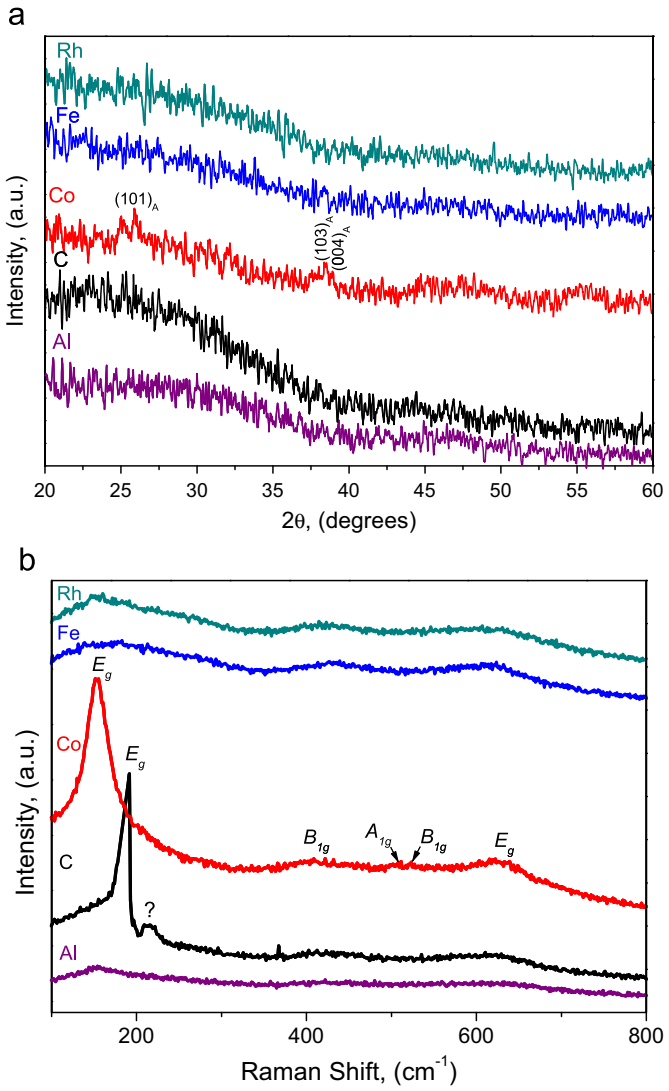

Fig. 3. (a)XRD and (b) Raman characterization of the as synthesized TiO_2 doped with Al, C, Co, Fe and Rh.

in our case by the presence of interstitial C atoms that interact with the lattice building up hydrostatic stresses. Based on the results in [32] the Raman shift in the $E_{g(2)}$ band correspond to approximately 50 kPa, presumably hydrostatic. Carbon is the only interstitial dopant in this work.

Other identifiable Raman bands in Fig. 3a for anatase are: E_g, B_{1g}, and the doublet A_{2g}. The E_g mode is identified by three bands (151, 193 and 630 cm^{-1}), while the B_{1g}, A_{1g} and B_{1g} are at 400, 508 and 512 cm^{-1} respectively [34]. None of the other bands are well resolved in any of the as synthesized samples. When anatase is nanostructured the E_g band shows a red shift (from 144 cm^{-1}) that is in agreement with our current and previous work [19,35]. In the case of the Co doped sample the corresponding grain size is ~5 nm that agrees with our previous work [1,2].

The heat treatments in all samples were conducted from 100 °C to 800 °C; although, to simplify this manuscript we focused in the most representative results (Fig. 4a and b)

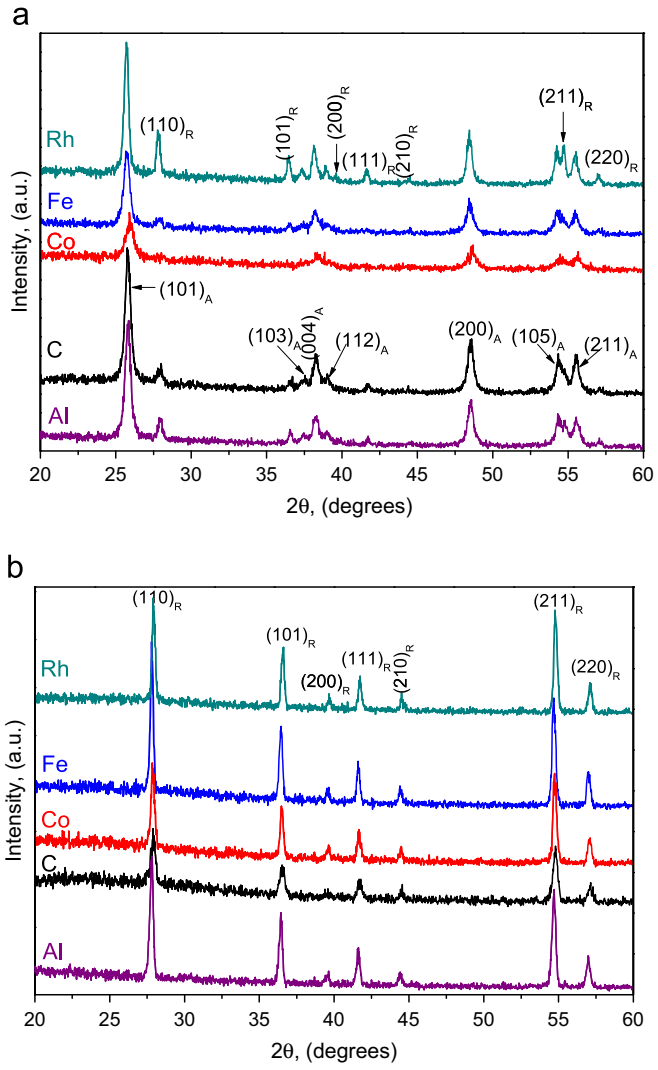

Fig. 4. XRD spectrum of doped TiO_2 heat treated at (a) 300 °C and (b) 800 °C.

the rest can be consulted in [30]. Selected XRD results for the heat treated samples at 300 °C and 800 °C are presented in Fig. 4. The XRD results at 300 °C do not show brookite that is attributed to a potential sensitivity of this phase to composition and lattice distortions. The sample with the smallest and wider peaks is the Co doped that seems to hinder the transformation to rutile and has the lowest crystal quality [26]. Samples heat treated at 800 °C show only rutile (Fig. 4b). Comparing the main reflections among anatase, $(101)_A$, and rutile, $(110)_R$, allows to conclude that rutile has larger grain size, crystal quality and seems to be a more rigid structure. This is concluded based on the characteristics of the XRD reflections from the respective structures. At the same time the stability of the reflections imply a limited potential for solid solutions.

The SEM micrographs of the as synthesized samples are presented in Fig. 5. From the SEM micrographs it can be observed that the doping has effects on the particle's characteristics that may affect their physicochemical properties. For instance the un-doped sample seems to be the densest of all the samples and has irregular morphology. The doped samples tend to be more globular with loose appearance. A qualitative analysis indicates the smallest particles are found in the Al and Co dope samples. This corresponds to the XRD results with wider and shorter reflections. The largest particles are found in pure TiO_2, Fe, Rh, and C doped samples.

The Raman characterization of the heat treated TiO_2 at 300 and 800 °C is given in Fig. 6a and b respectively. Both figures show that anatase is the first transforming phase followed by rutile confirming the XRD results. In the spectrums can be identified the presence of the E_g, B_{1g}, A_{1g}, bands for anatase. It is also important to mention that Al, C, Co and Fe enhance the E_g band. We attribute this effect to a surface enhancing phenomena [37,38] along with a mid to long range crystalline structure. Similar effects were reported on TiO_2 doped with Zn [38]. Rutile peaks are evident in the Rh and Co doped samples; in fact, in the Rh case rutile dominates the spectrum except for the $E_{g(1)}$ and $E_{g(2)}$ bands. Therefore, anatase is identified by a low intensity E_g band. Comparing Raman and XRD results is clear that anatase is the predominant phases on the sample; therefore, Rh may not have the same enhancing effect on anatase as the other dopants. Rh actually prevents the clear observation of anatase bands.

Fig. 6b presents the TiO_2 doped samples heat treated at 800 °C. In all cases the predominant component is rutile. The intensity of the Raman signal for the Fe and Rh doped is weaker than that seeing in the Al, C and Co doped samples. This is attributed to the doping on TiO_2 that prevents a clear visualization of the vibrational modes of rutile. Although, the following rutile bands can be identified B_{1g}, E_g, and A_{1g} and correspond to those reported in [39]. The above bands are observed at 235, 270, 259 and 685 cm^{-1} and correspond to second scattering features and they do not have fundamental vibrational significance [40]. The two bands at 567 and 685 cm^{-1} are disordered deactivated bands that are sensitive to grain size. The red shift of the E_g and A_{1g} bands can be used to determine the grain size on rutile; however, careful considerations are needed [40,41]. Therefore, we reported only the XRD-Scherer results.

The inset in Fig. 6b shows that all the TiO_2 doped samples have a clearly defined E_g band; except for the Rh doped sample showing a blue shift. These combination of factors are common of a nanostructured anatase and is in agreement with the results presented herein and previous reports [42]. The disagreement among the XRD and the Raman for the Fe and Rh samples is attributed to the precipitation of the dopant along the surface of the TiO_2 particles that are absorbing or preventing the Raman scattering. Previous reports indicate that the surface particles are oxides, Rh_2O_3 likely [43]. The nanostructured Rh_2O_3 particles act as quantum sites (q-sites) behaving as electron holes effects, traps or both [43].

The grain size determination for anatase and rutile is presented in Fig. 7. Previous reports indicate that when

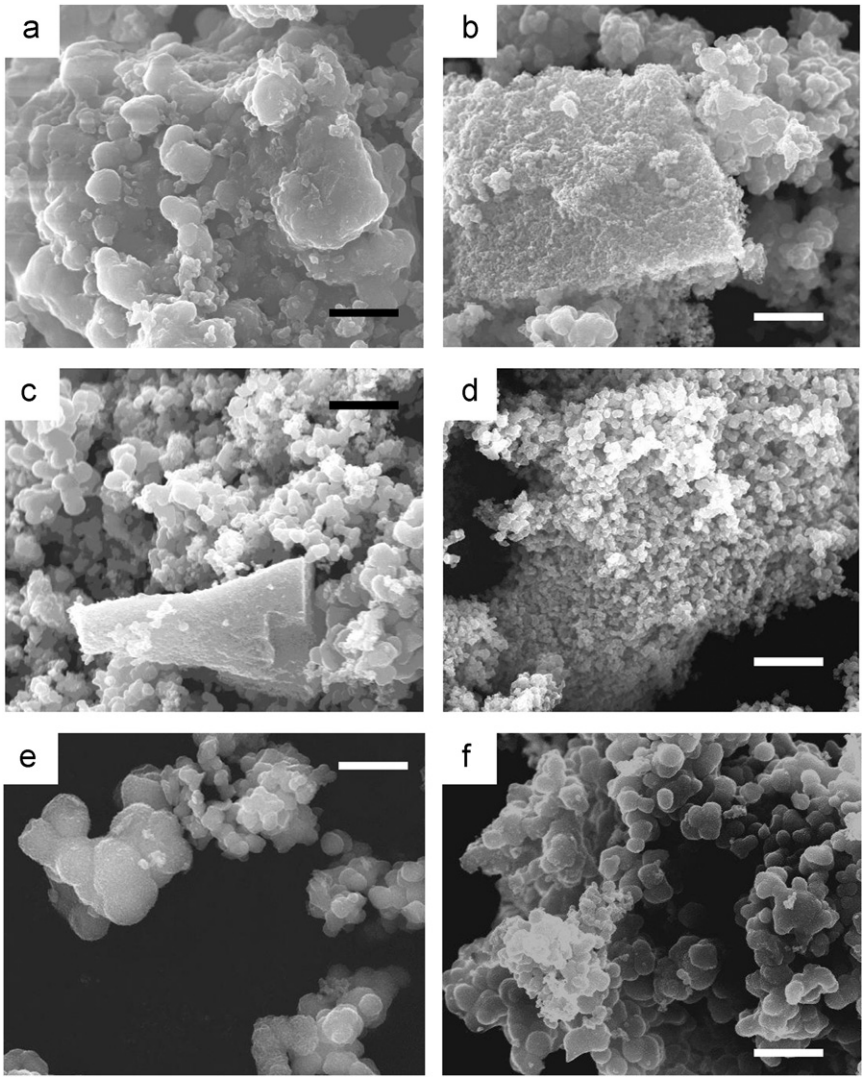

Fig. 5. SEM micrographs of the as synthesized powders for the un-doped (a) and doped (b–f) samples. The SEM micrographs correspond to the following dopants (b) Al, (c) C, (d) Co, (e) Fe and (f) Rh. The scale represents 10 μm.

sonochemically synthesized pure TiO_2 is heat treated above 500 °C the anatase particles experience a coarsening that is followed by a grain size reduction [1,2]. Rutile coarsens continuously in an exponential-like fashion. In Fig. 7a it is clear that larger anatase grains are usually found at temperatures between 100 and 200 °C and in all cases the grain size decreases. In addition, the anatase grains are in all cases smaller than 21 nm that is below the range previously reported [1,2,20]. The average grain size of rutile is relatively larger (Fig. 7b), but it is still smaller than reported values [2]. This is attributed to sonication that allows the synthesis of smaller particles and doping precipitation prevents coarsening. Carbon doped samples have a grain size below 12 nm at temperatures of 400 °C. The coarsening observed in rutile is unpredictable and does not obey an exponential growth as seen for reported in [2].

Fig. 8 shows the fraction transforming anatase–rutile. The transformation temperatures from anatase–rutile occur at unusually low temperatures. For instance, in the case of Rh doped samples anatase synthesizes at 100 °C. Carbon doping allows the synthesis of rutile at temperatures as low as 200 °C and fully transformed to rutile below 400 °C. The opposite is observed in the Al and Co samples where the transformation to rutile is completed above 500 °C that is previously reported [1,2]. Therefore, it can be concluded that C, Rh, and Fe are anatase and rutile promoters; while, Co and Al does not have clear effects on transformation temperature.

The X-ray photoelectron spectroscopy (XPS) is used to determine the electronic state and fractions of the elements present in the investigated samples. In all cases the ratio Ti:O is approximately 1:2 suggesting a TiO_2 stoichiometry. In the as synthesized powder, the dopant is well dispersed within the TiO_2 particles. Table 2 shows the concentration of the doping elements and how they change with heat treatment temperatures. The increase in dopant concentration implies a diffusion of the dopant elements to the particle's surface where they precipitate. The high affinity

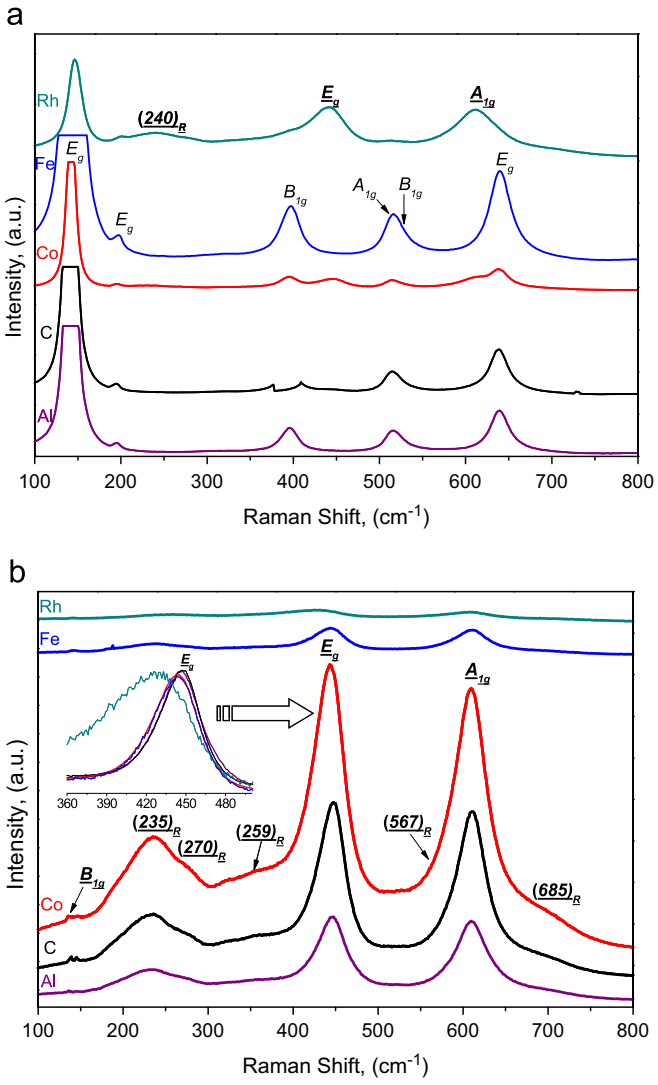

Fig. 6. Raman characterization of the TiO_2 heat treated at (a) 300 °C and (b) 800 °C doped with Al, C, Co, Fe and Rh.

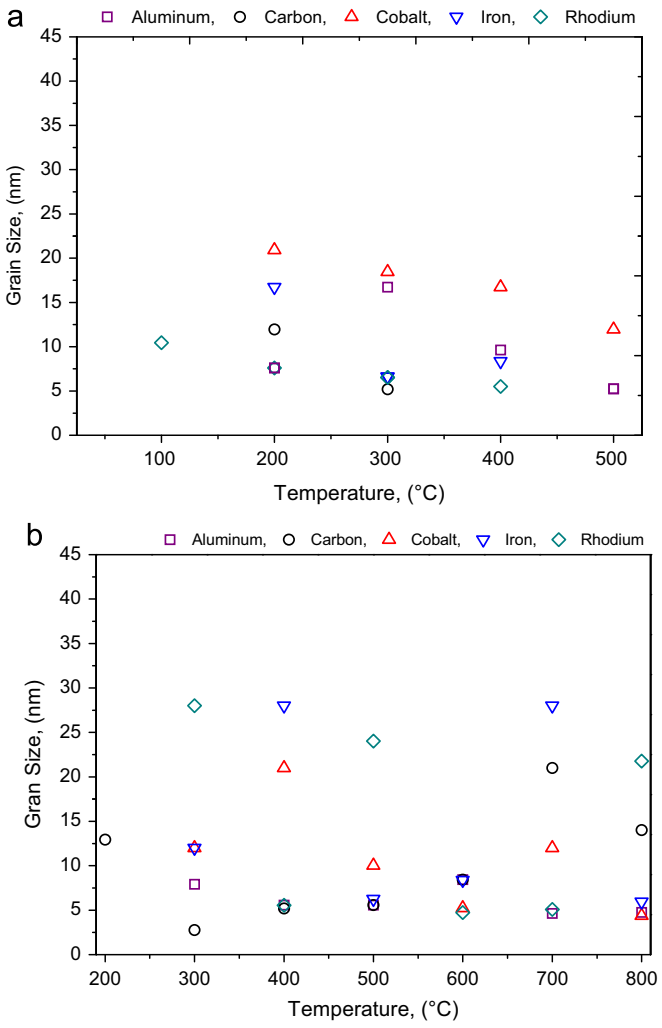

Fig. 7. Grain size determination for TiO_2 doped with Al, C, Co, Fe and Rh. The grain size results correspond to anatase (a) and rutile (b) at different heat treatment temperatures.

among Ti and oxygen prevents their combination with other elements making a rigid structure and forcing the dopants to diffuse out of the TiO_2 particles.

In the XPS results show that the locations of the Ti $2p_{1/2}$ doublets are at 465 eV and 459 eV with a separation of approximately 5.7 eV. This indicates a +4 oxidation state. No doublets for the presence of Ti^{2+} and Ti^{3+} are identified, confirming the TiO_2 stoichiometry. This condition is common in all the investigated samples (see Table 2) and agrees with previous reports [44]. The *C* doped results are not presented because carbon results were unusually higher than expected that is attributed to external contamination. Potential source of *C* contamination include: (i) handling and (ii) traces of carbon from the titanium isopropoxide. The lower Ti $2p_{1/2}$ values in the Co, Fe and Rh doped and heat treated at 800 °C suggest that the dopant is in the surface forming oxides. This is expected because the heat treatments conditions can favor these reactions.

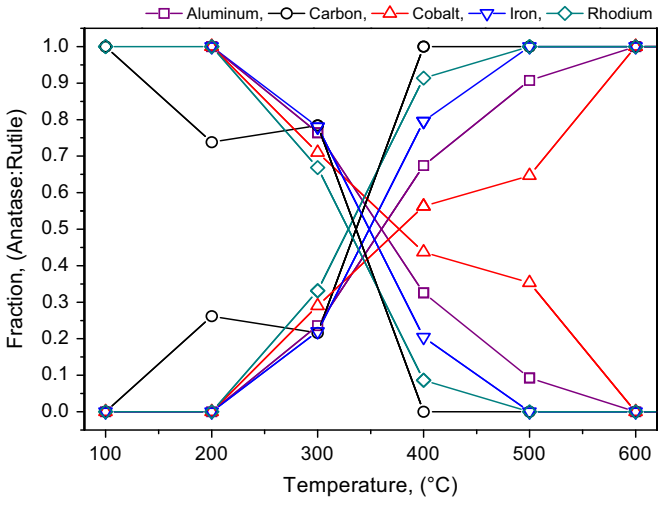

Fig. 8. Fraction of anatase and rutile for the doped samples. The fractions was calculated with a modified version of Spur-Meyer's Equations [30].

Table 2
X-ray Photoelectron Spectroscopy (XPS) results of the as synthesized and doped TiO_2.

Dopant	Temperature (°C)	Phases	Ti 2p (at%)	O 1s (at%)	Dopant (at%)
Non doped	Synthesized	Amorphous	28.6	71.4	N/A
Aluminum (2p)	200	Anatase	30.9	67.8	1.3
	300	Anatase+Rutile	29.3	70.5	0.2
	800	Rutile	21.0	71.2	7.8
Cobalt (2p)	Synthesized	Amorphous	29.1	70.7	0.2
	100	Anatase	31.5	68.3	0.2
	200	Anatase	30.5	69.2	0.3
	400	Anatase+Rutile	28.7	70.9	0.4
	800	Rutile	16.4	80.9	2.7
Iron (2p)	200	Anatase	31.3	68.6	0.1
	300	Anatase+Rutile	30.8	68.3	0.9
	800	Rutile	25.8	71.1	3.1
$Rhodium_{0.075}$ (3d)	200	Anatase	30.9	68.8	0.3
	300	Anatase+Rutile	29.2	70.4	0.4
	800	Rutile	26.9	72.7	0.4
$Rhodium_{0.15}$ (3d)	200	Anatase	31.4	68.4	0.2
	300	Anatase+Rutile	30.3	69.2	0.5
	800	Rutile	16.8	80.1	3.1

The theoretical values for anatase and rutile are: anatase, $a=3.7842$ nm, $c=9.5143$ nm and rutile, are: $a=4.5937$ nm, and $c=2.9587$ nm [45,46]. The lattice parameters (a, c) and volumes were calculated based on the XRD results. A comparison of these values with our results is presented in Fig. 9. The results were normalized to minimize the systematic error in the XRD system against the theoretical values. The lattice parameters for rutile were normalized against the carbon doped sample that is the first sample transforming to rutile.

The as synthesized samples show differences in lattice parameter for anatase "a" of $0.72 \pm 0.20\%$, and "c" of $1.50\% \pm 0.55\%$. For rutile the differences are: $a=1.57 \pm 0.46\%$ and $c=1.15 \pm 0.29\%$. In the heat treated samples the average differences are: $a=0.88 \pm 0.15\%$ and $c=1.85 \pm 0.36\%$ for anatase and for rutile, $a=1.69 \pm 0.27\%$, $c=1.24 \pm 0.21\%$. For anatase, "a" increases with temperature in the 300–400 °C range. At 500 °C the Al and Co doped samples show a decrease in lattice parameter similar to that observed in the pure sample demonstrating that their solubility is practically negligible. The XRD results show that rutile has more rigid lattices due to its stable lattice parameter with rather poor potential to form solid solutions. Although, the solubility of the dopants in TiO_2 is low; anatase may dissolve more dopant because it has larger interstitials [47]. However, solid solutions are not expected.

Fig. 10 illustrates the band gap values for the investigated samples in as synthesized and heat treated conditions. The band gap for the pure TiO_2 is relatively lower (2.8 eV) that commercial anatase (3.0–3.2 eV [48]); however, it reaches similar values after heat treated at temperatures as low as 100 °C. Based on Figs. 2 and 4 pure TiO_2 is the only sample where brookite is present and may have a direct contribution to band gap [31]. The band gap can be manipulated in synthesized and selected samples heat treated at temperatures 200 °C or above 700 °C. Samples heat treated from 200 to 600 °C have band gaps similar to anatase [20,49].

The Co, Al and $Rh_{0.075}$[3] doped samples show band gaps comparable to that of commercial anatase and are relatively constant for heat treated samples of up to 600 °C. Higher temperatures widen their band gaps. The opposite behavior is observed in the as synthesized Fe and C doped samples with wider band gaps: 3.94 and 4.17 eV respectively. The heat treated (100–600 °C) C doped sample has a relatively constant band gap of 3.27 ± 0.11 eV. Higher temperatures result in band gap values similar to those reported for rutile. To a naked eye the Al doped powders are white, while the Rh, Co and Fe doped powders are red.

The band gap in Fe doped samples show an unusual increase in heat treated samples at 200 and 300 °C (3.69 and 3.67 eV respectively). These changes are followed by a decrease to 3.2 ± 0.06 eV through 600 °C. This sudden increase is attributed to the transformation from magnetite (Fe_3O_4) to maghemite (γ-Fe_2O_3) between 200 and 300 °C followed by a subsequent transformation to hematite (α-Fe_2O_3) above 300 °C [50].

Fig. 11a and b shows HRTEM micrographs of TiO_2 particles dope with Co and Rh respectively. Both micrographs correspond to samples heat treated at 800 °C. There are two types of particles that are clearly distinguishable in size; the smaller ones correspond to the dopant as identified by their characteristic d-spacing and crystalline structure (see insets). The dopants form precipitates with q-site characteristics that are shown in the right hand insets with their respective d-spacing and crystallographic characteristics. The larger particles correspond to rutile. The precipitates decorate the TiO_2 particles with q-sites as previously identified in the literature [43]. This confirms the XRD, Raman and XPS results where is indicated that the dopants diffuse out of the TiO_2 lattice and precipitates at the surface's particles. The HRTEM results indicates (Fig. 11a) that the analyzed particle has a rock salt structure similar to that of CoO stoichiometry as previously reported [51]. The Rh is in the form of Rh_2O_3 precipitates with hexagonal crystalline structure as seen in the respective inserts.

4. Discussions

The phase identification conducted by thermal analysis is in good agreement with the XRD and Raman results. The recorded temperatures during thermal analysis are relatively lower compared to previously reported values. This behavior is attributed this to two main factors: (i)

[3]The 0.075 sub index indicates the at% of Rh added to the corresponding sample.

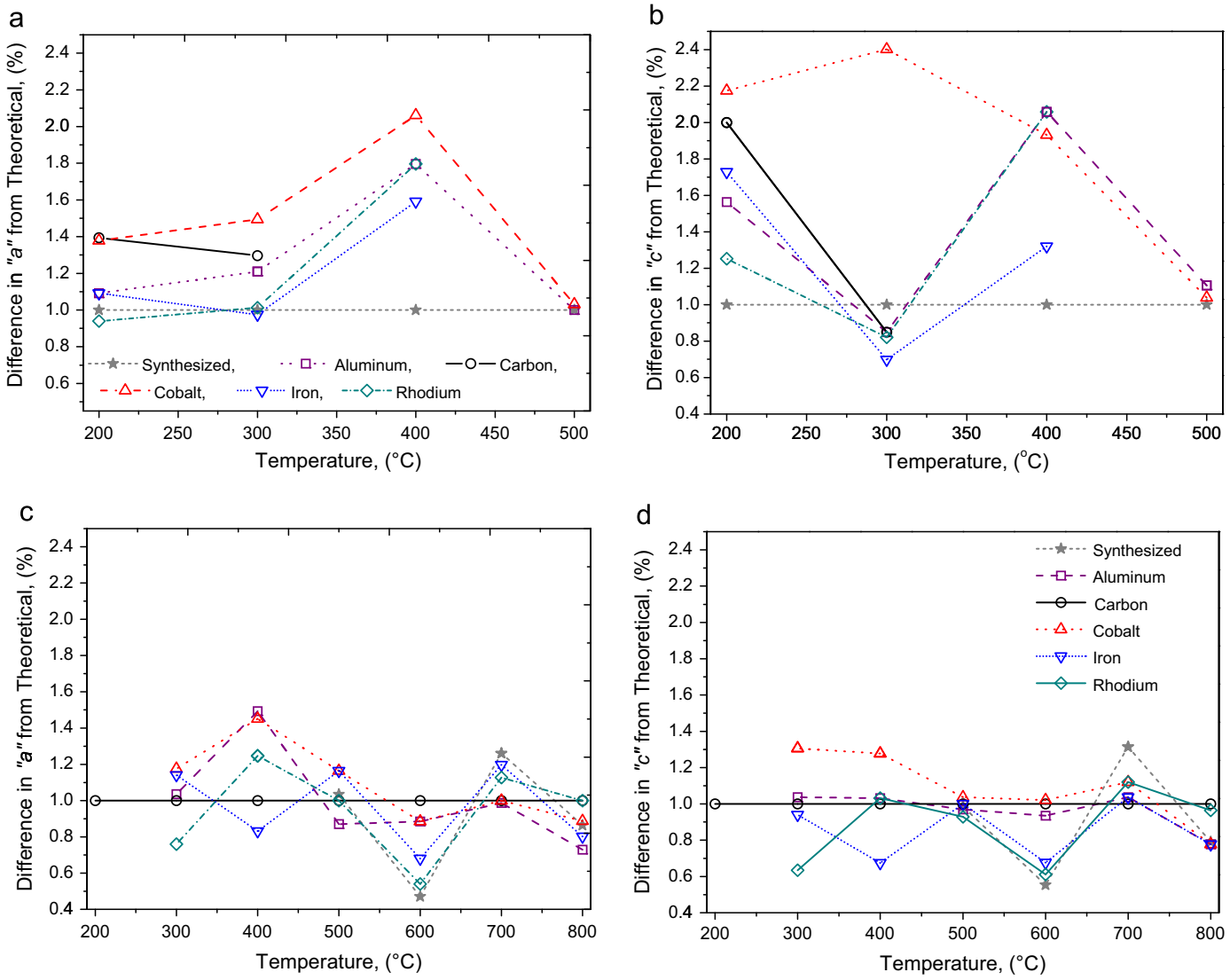

Fig. 9. Comparison among lattice parameters for (a,b) anatase and (c,d) rutile in the as synthesized and heat treated forms. The comparison was made against the values reported in [45,46]. Notice that the differences in lattice parameter (with respect to the theoretical) is larger for anatase when compared to that of rutile; further, C promote the transformation to anatase more rapidly than the other elements and seems to stabilize the lattice parameter "*c*".

sono-synthesis/grain size and (ii) doping. The as synthesized samples are quasi-amorphous, except for those doped with Co. All samples, but pure TiO_2, develop a bi-crystal framework when heat treated between 100 and 600 °C. Pure TiO_2 presents a tri-crystal framework between 100 and 300 °C followed by a bi-crystal arrangement at temperatures below 600 °C. The only interstitial dopant is carbon and sponsors the rapid transformation to rutile at temperature as low as 200 °C. In Raman the C doped sample present only the $E_{g(2)}$ band for anatase that is well resolved and sharp. These characteristics are typical of residual stresses in the TiO_2 lattice and are attributed to the interstitial interactions of C.

The transition temperatures to anatase and rutile are characteristic for each dopant. The following is the order in which each sample transforms to anatase–rutile: C, Rh, Fe, Al and Co. Co does not seem to influence the transformation to rutile. The grain size of all the heat treated samples is below 30 nm for rutile and 20 nm for anatase and there is no correlation among temperature and grain size. The XRD results indicate limited interaction among the TiO_2 and dopant. No other phases were identified and no significant changes in lattice parameters were identified. This suggests that the rigidity of the TiO_2 lattices prevents substitutional diffusion and force the dopants to diffuse out and precipitate along the particle's surface. The precipitates prevent grain growth and stabilize their size by hindering coarsening as demonstrated by the Scherrer results. The increase in dopant concentration with temperature reported by XPS is attributed to surface precipitation.

The Raman, XRD and XPS results demonstrate that in the as synthesized samples the dopants are dispersed or dissolved within the TiO_2 lattice containing a high density of defects. As the heat treatment temperatures increase the crystal quality index of TiO_2 increases and the structure

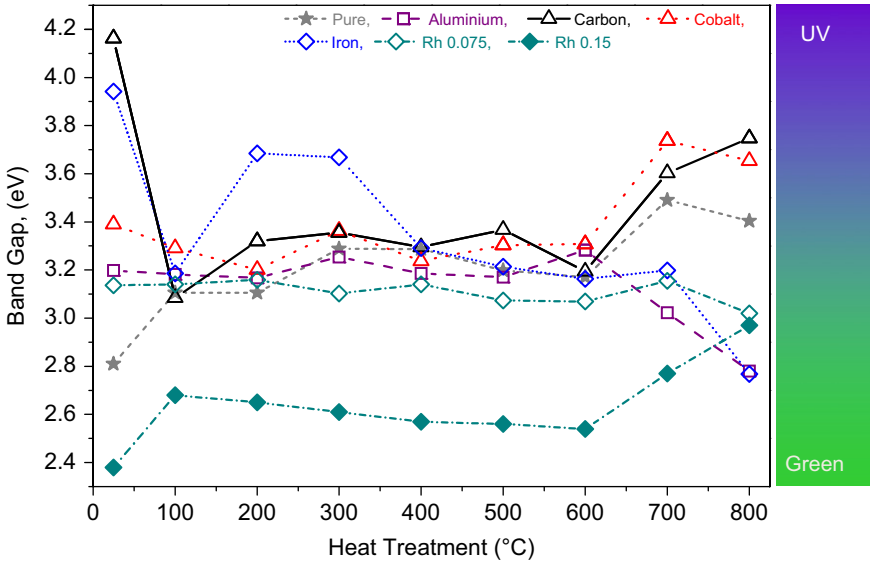

Fig. 10. Band gap of as synthesized samples pure TiO_2 and doped samples using Al, C, Co, Fe, and Rh. The results presented are for the as synthesized samples as well as for the heat treated. The scale on the right shows the approximate colors corresponding to the respective band gap values. (For interpretation of the references to color in this figure legend, the reader is referred to the web version of this article.)

becomes more rigid. This force the dopants to diffusion out of the TiO_2 lattice and permit their precipitation along the TiO_2 surface. This is observed by the increasing concentration of the dopant with heat treatment temperature (Table 2). Some of the investigated samples show a reduced intensity in their characteristic Raman bands, which is unexpected. This is explained by the presence of the precipitates along the TiO_2 particles that prevents an effective Laser/Raman signal interaction. This effect is clearly demonstrated by HRTEM with the nanoparticles of Rh_2O_3 and CoO.

The precipitates in the surface of the TiO_2 particles are nanostructured and well dispersed. The TiO_2 is well known for its catalytic character; however, its catalytic activity can be enhanced by the observed *q*-sites [43,52]. The *q*-sites may generate plasmonic effects that enhance their activity [53]. Under certain conditions the Rh_2O_3 is a p-type semiconductor with high conductivity and is magnetic at room temperature [54]. The CoO is a semi-conductor [51]. The plasmonic effect occurs if the particles meet specific size, shape, electrical characteristics and distribution as indicated in Ref. [53]. The precipitates observed in the investigated samples (Fig. 11) meet the requirements reported in [53]. Therefore, the reduction in the band gap (to 2.38 eV) in TiO_2 can be the results of combined effects; namely, grain size and physicochemical nature of the precipitates. The band gap reduction make some of the doped anatase active in green light. Previous work reports comparable effects; however, the dopant concentration is significantly larger [16,43,49]. The effectiveness in our work is attributed to our sono-synthesis and the controlled heat treatments that permit the formation of *q*-sites [53].

In the as synthesized conditions the band gap for the C and Fe doped samples is wider than that previously reported. The opposite behavior is observed in the pure TiO_2 and $Rh_{0.15}$ doped sample, while Al, Co and $Rh_{0.075}$ does not seem to have major effects. The heat treated samples, but $Rh_{0.15}$, have a relatively constant band gap of approximately 3.21 ± 0.09 eV that is typical of anatase. Increasing the Rh additions from 0.075 to 0.15 at% decreases the band gap from 2.97 to 2.38 eV in as synthesized and heat treated at 800 °C respectively.

Heat treated samples at 800 °C have single crystal framework (rutile) without apparent coarsening (Fig. 7), but variable band gap. For instance, the pure TiO_2, C, Co and $Rh_{0.15}$ doped have a wider band gap and the other samples present a narrower band gap. These changes indicate that crystal framework is responsible for band gap modifications. This is contrary to the idea that grain size has a direct effect on band gap. Therefore, the crystal framework is the most efficient mechanism to control the band gap.

For low temperature applications (below 100 °C) C and Fe doping are ideal to increase the band gap, while pure and $Rh_{0.15}$ decrease the band gap. Heat treated pure TiO_2 or doped is recommended when stable band gap are required in working environments below 600 °C. For working environments exceeding 600 °C the dopant must be selected depending on the needs. For example, the band gap in Al and Fe doped samples decreases to values of approximately 2.7 eV that are comparable to that observed in the $Rh_{0.15}$ sample. If lower band gaps are needed $Rh_{0.15}$ is the alternative, but limits its working temperature below 100 °C or less. For wide band gap applications the recommendations for low temperatures are C and Fe doped and for high temperature (above 600 °C) pure TiO_2, C and Co doped are suggested. The variety of band gaps in the investigated samples allows to produce catalytic materials active in a wide range of the visible spectrum from the green (522 nm) to the UV (297 nm). Rutile is

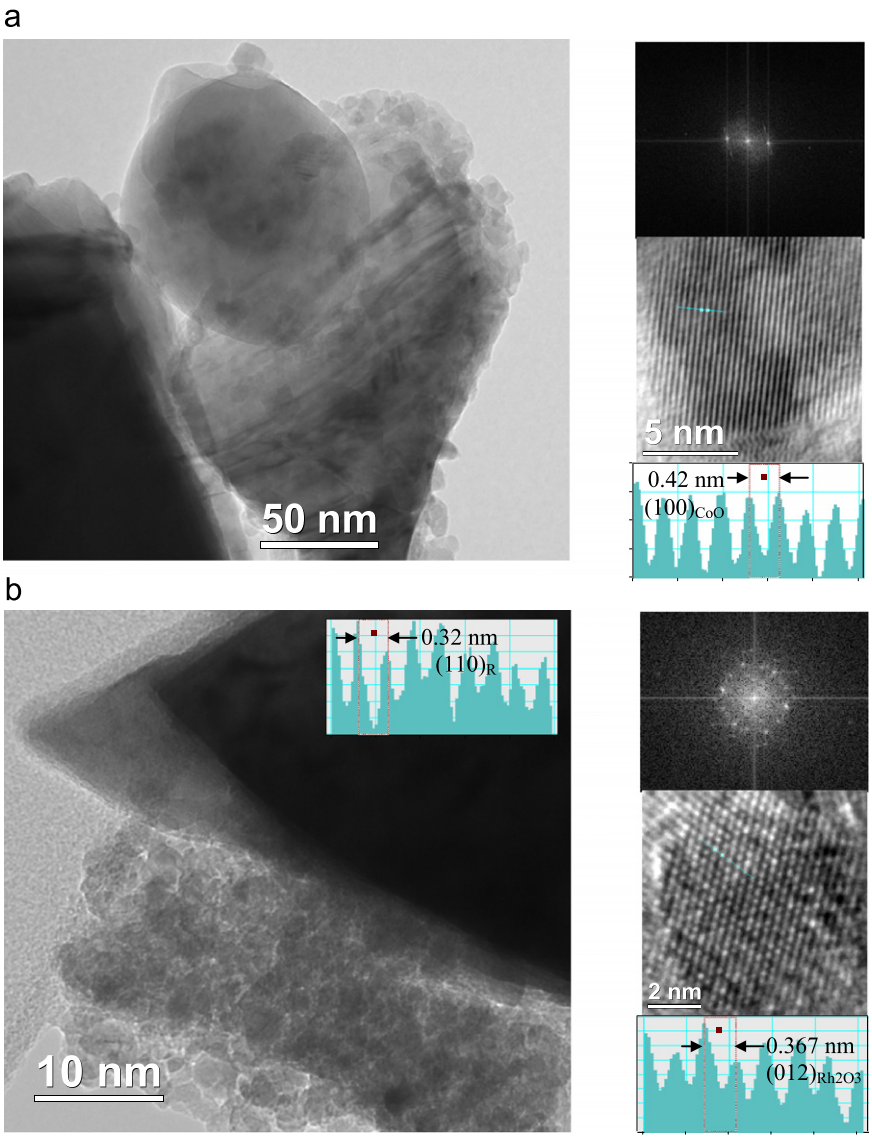

Fig. 11. HRTEM images of the Co (a) and Rh (b) doped samples and heat treated at 800 °C. The insets on the right are showing HRTEM and its respective FFT-diffraction pattern of a particle (*Q*-sites) precipitate at the surface of a TiO_2 crystal. Note that the larger particles are TiO_2 showing a decoration of Co and Rh oxides. The histograms in the insets are showing the interatomic distances for the respective phases (R = rutile, CoO = cobalt oxide and Rh_2O_3 = rhodium oxide). The lattice parameters were compared against the following references [47,51,55].

more stable than anatase and with the right doping and heat treatment rutile may be more useful for extreme environments (e.g. aerospace) than anatase.

5. Conclusions

Thermal analysis can be used to detect phase transformations on TiO_2 (e.g. anatase, brookite and rutile). Sonication is an ideal method to dope TiO_2 during the synthesis producing nanostructured particles of quasi-amorphous TiO_2 that can be transformed in a controlled way into pure anatase, rutile, bi/tri-crystal frameworks. Brookite was observed only in pure TiO_2. As synthesized TiO_2 tend to decrease its band gap in its pure and $Rh_{0.15}$ doped form, while C and Fe widen the band gap. The crystal framework (anatase, brookite, rutile, or mixes) has the strongest effect on band gap, over dopant and grain size. Sonicated samples are sensitive to transform to anatase and rutile at relatively low temperatures. The band gap reduction; hence catalytic activity, is affected by the precipitates (*q*-sites) forming along the surface of TiO_2 particles. Sono-chemically synthesized TiO_2 is catalytically active in the visible spectrum ranging from UV (297 nm) to the green (522 nm).

Acknowledgments

The authors would like to thank the University of Houston and the State of Texas for their invaluable support through the Star Up, Small grant and HEAFS funding.

References

[1] F.C. Robles Hernandez, L. Gonzalez-Reyes, I. Hernandez-Perez, Effect of coarsening of sonochemical synthesized anatase on BET surface characteristics, Chemical Engineering Science 66 (4) (2011) 721–728.

[2] L. Gonzalez-Reyes, I. Hernandez-Perez, F.C.R. Hernandez, H.D. Rosales, E.M. Arce-Estrada, Sonochemical synthesis of nanostructured anatase and study of the kinetics among phase transformation and coarsening as a function of heat treatment conditions, Journal of the European Ceramic Society 28 (8) (2008) 1585–1594.

[3] U. Diebold, The surface science of titanium dioxide, Surface Science Reports 48 (5-8) (2003) 53–229.

[4] H. Arami, M. Mazloumi, R. Khalifehzadeh, S.K. Sadmezhaad, Sonochemical preparation of TiO_2 nanoparticles, Materials Letters 61 (23-24) (2007) 4559–4561.

[5] W.L. Guo, Z.M. Lin, X.K. Wang, G.Z. Song, Sonochemical synthesis of nanocrystalline TiO2 by hydrolysis of titanium alkoxides, Microelectronic Engineering 66 (1-4) (2003) 95–101.

[6] J.C. Yu, L.Z. Zhang, J.G. Yu, Direct sonochemical preparation and characterization of highly active mesoporous TiO2 with a bicrystalline framework, Chemistry of Materials 14 (11) (2002) 4647–4653.

[7] K.S. Suslick, G.J. Price, Applications of ultrasound to materials chemistry, Annual Review of Materials Science 29 (1999) 295–326.

[8] K.S. Suslick, Applications of ultrasound to materials chemistry, MRS Bulletin 20 (4) (1995) 29–34.

[9] M.R. Hoffmann, S.T. Martin, W.Y. Choi, D.W. Bahnemann, Environmental Applications of Semiconductor Photocatalysis, Chemical Reviews 95 (1) (1995) 69–96.

[10] R.X. Cai, Y. Kubota, T. Shuin, H. Sakai, K. Hashimoto, A. Fujishima, Induction of cytotoxicity by photoexcited TiO_2 particles, Cancer Research 52 (8) (1992) 2346–2348.

[11] J.Y. Gan, Y.C. Chang, T.B. Wu, Dielectric property of $(TiO_2)_{(x)} - (Ta_2O_5)_{(1-x)}$ thin films, Applied Physics Letters 72 (3) (1998) 2346–2348.

[12] A. Fujishima, X.T. Zhang, Titanium dioxide photocatalysis: present situation and future approaches, Comptes Rendus Chimie. 9 (5-6) (2006) 750–760.

[13] J.H. Braun, Titanium dioxide—A review, Journal of Coatings Technology 69 (868) (1997) 59–72.

[14] N.I. Al-Salim, S.A. Bagshaw, A. Bittar, T. Kemmitt, A.J. McQuillan, A.M. Mills, M.J. Ryan, Characterisation and activity of sol–gel-prepared TiO_2 photocatalysts modified with Ca, Sr or Ba ion additives, Journal of Materials Chemistry 10 (10) (2000) 2358–2363.

[15] S. Ito, S. Inoue, H. Kawada, M. Hara, M. Iwasaki, H. Tada, Low-temperature synthesis of nanometer-sized crystalline TiO_2 particles and their photoinduced decomposition of formic acid, Journal of Colloid and Interface Science 216 (1) (1999) 59–64.

[16] M. Hirano, C. Nakahara, K. Ota, M. Inagaki, Direct formation of zirconia-doped titania with stable anatase-type structure by thermal hydrolysis, Journal of the American Ceramic Society 85 (5) (2002) 1333–1335.

[17] A.J. Maira, K.L. Yeung, C.Y. Lee, P.L. Yue, C.K. Chan, Size effects in gas-phase photo-oxidation of trichloroethylene using nanometer-sized TiO_2 catalysts, Journal of Catalysis 192 (1) (2000) 185–196.

[18] C.K. Chan, J.F. Porter, Y.G. Li, W. Guo, C.M. Chan, Effects of calcination on the microstructures and photocatalytic properties of nanosized titanium dioxide powders prepared by vapor hydrolysis, Journal of the American Ceramic Society 82 (3) (1999) 566–572.

[19] A.K.P.D. Savio, D. Starikov, A. Bensaoula, R. Pillai, L.L. de la Torre García, F.C. Robles Hernández, Tunable TiO_2 (anatase and rutile) materials manufactured by mechanical means, Ceramics International 38 (5) (2012) 3529–3535.

[20] L. González-Reyes, I. Hernández-Pérez, L. Díaz-Barriga Arceo, H. Dorantes-Rosales, E. Arce-Estrada, R. Suárez-Parra, J.J. Cruz-Rivera, Temperature effects during Ostwald ripening on structural and bandgap properties of TiO_2 nanoparticles prepared by sonochemical synthesis, Materials Science and Engineering: B 175 (1) (2010) 9–13.

[21] F.C. Robles Hernandez, J.H. Sokolowski, Thermal analysis and microscopical characterization of Al–Si hypereutectic alloys, Journal of Alloys and Compounds 419 (1-2) (2006) 180–190.

[22] F.C. Robles Hernandez, J.H. Sokolowski, Effects and on-line prediction of electromagnetic stirring on microstructure refinement of the 319 Al–Si hypoeutectic alloy, Journal of Alloys and Compounds 480 (2) (2009) 416–421.

[23] F.C. Robles Hernandez, J.A. Neal, U.S. Aldea, Thermal characterization of poultry for the development of a comprehensive device to monitor safety and proper coking, Journal of Food Process Engineering, http://dx.doi.org/10.1111/j.1745-4530.2011.00665.x, in press.

[24] J.F. Eberth, J.A. Neal, F.C. Robles Hernandez, Evaluation of heat propagation through poultry in a reduced computational-cost model of contact cooking, International Journal of Food Science and Technology 47 (2012) 1130–1137.

[25] R.O. Olivares, C.I. Garcia, A. DeArdo, S. Kalay, F.C.R. Hernandez, Advanced metallurgical alloy design and thermomechanical processing for rails steels for North American heavy haul use, Wear 271 (1-2) (2011) 364–373.

[26] B.D. Cullity, Elements of X-ray diffraction, 2nd ed., Addison-Wesley Pub. Co., Reading, Mass, 1978.

[27] E.J. Lavernia, Z. Zhang, F. Zhou, On the analysis of grain size in bulk nanocrystalline materials via X-ray diffraction, Metallurgical and Materials Transactions A 34A (6) (2003) 1349–1355.

[28] M.A. Zanjanchi, H. Noei, M. Moghimi, Rapid determination of aluminum by UV–vis diffuse reflectance spectroscopy with application of suitable adsorbents, Talanta 70 (5) (2006) 933–939.

[29] F.C. Robles Hernandez, J.H. Sokolowski, Comparison among chemical and electromagnetic stirring and vibration melt treatments for Al–Si hypereutectic alloys, Journal of Alloys and Compound 426 (1-2) (2006) 205–212.

[30] A.K.P.D. Savio, Characterization Protocol for Titanium dioxide (Anatase: Rutile) Use for Photocatalytic Applications, in: Mechanical Engineering Technology, Vol. Master of Science, University of Houston, Houston, 2011, pp. 158.

[31] R. Zallen, M.P. Moret, The optical absorption edge of brookite TiO_2, Solid State Communications 137 (3) (2006) 154–157.

[32] T. Ohsaka, S. Yamaoka, O. Shimomura, Effect of Hydrostatic-Pressure on the Raman-Spectrum of Anatase (Tio_2), Solid State Communications 30 (6) (1979) 345–347.

[33] V. Swamy, Size-dependent modifications of the first-order Raman spectra of nanostructured rutile $TiO_{(2)}$, Physical Review B 77 (19) (2008) 195414–195414.

[34] U. Balachandran, N.G. Eror, Raman-spectra of titanium-dioxide, Journal of Solid State Chemistry 42 (3) (1982) 276–282.

[35] P.P. Lottici, D. Bersani, M. Braghini, A. Montenero, Raman-scattering characterization of gel-derived titania glass, Journal of Materials Science 28 (1) (1993) 177–183.

[37] R. Aroca, S. RodriguezLlorente, Surface-enhanced vibrational spectroscopy, Journal of Molecular Structure 408 (1997) 17–22.

[38] L. Yang, Y. Zhang, W. Ruan, B. Zhao, W. Xu, J.R. Lombardi, Improved surface-enhanced Raman scattering properties of TiO_2 nanoparticles by Zn dopant, Journal of Raman Spectroscopy 41 (7) (2010) 721–726.

[39] S.P.S. Porto, P.A. Fleury, T.C. Damen, Raman Spectra of Tio_2,Mgf_2,Znf_2,Fef_2,and Mnf_2, Physical Review 154 (2) (1967) 522–526.

[40] V. Swamy, B.C. Muddle, Q. Dai, Size-dependent modifications of the Raman spectrum of rutile $TiO_{(2)}$, Applied Physics Letters 89 (16) (2006) 163118–163118.

[41] T. Mazza, P. Milani, Comment on "Size-dependent modifications of the Raman spectrum of rutile $TiO_{(2)}$" Applied Physics Letters 89, art no 163118 (2006); Applied Physics Letter 91 (4) (2007).

[42] C.T. Williams, E.K.Y. Chen, C.G. Takoudis, M.J. Weaver, Reduction kinetics of surface rhodium oxide by hydrogen and carbon monoxide at ambient gas pressures as probed by transient surface-enhanced Raman spectroscopy, Journal of Physical Chemistry B 102 (24) (1998) 4785–4794.

[43] W.Y. Choi, A. Termin, M.R. Hoffmann, The role of metal-ion dopants in quantum-sized Tio_2—Correlation between photoreactivity and charge-carrier recombination dynamics, Journal of Physical Chemistry—USA 98 (51) (1994) 13669–13679.
[44] G.M. Liu, W. Jaegermann, J.J. He, V. Sundstrom, L.C. Sun, XPS and UPS characterization of the TiO_2/ZnPcGly heterointerface: Aligmment of energy levels, Journal of Physical Chemistry B 106 (23) (2002) 5814–5819.
[45] C.J. Howard, T.M. Sabine, F. Dickson, Structural and thermal parameters for rutile and anatase, Acta Crystallographica B 47 (1991) 462–468.
[46] M. Horn, C.F. Schwerdtfeger, E.P. Meagher, Refinement of the structure of anatase at several temperatures*, Zeitschrift für Kristallographie. 136 (3-4) (1972) 273–281.
[47] D.T. Cromer, K. Herrington, The structures of anatase and rutile, Journal of the American Chemical Society 77 (18) (1955) 4708.
[48] T.P. Ang, J.Y. Law, Y.F. Han, Preparation, characterization of sulfur-doped nanosized $TiO_{(2)}$ and photocatalytic degradation of methylene blue under visible light, Catalysis Letters 139 (1-2) (2010) 77–84.
[49] A. Amtout, R. Leonelli, Optical properties of rutile near its fundamental band gap, Physical Review B, Condensed Matter 51 (11) (1995) 6842–6851.
[50] S. Franger, P. Berthet, O. Dragos, R. Baddour-Hadjean, P. Bonville, J. Berthon, Large influence of the synthesis conditions on the physico-chemical properties of nanostructured Fe_3O_4, Journal of Nanoparticle Research 9 (3) (2007) 389–402.
[51] R.W. Grimes, K.P.D. Lagerlof, Polymorphs of cobalt oxide, Journal of the American Ceramic Society 74 (2) (1991) 270–273.
[52] H.W. Peng, J.B. Li, S.S. Li, J.B. Xia, First-principles study on rutile TiO_2 quantum dots, Journal of Physical Chemistry C 112 (36) (2008) 13964–13969.
[53] J.A. Scholl, A.L. Koh, J.A. Dionne, Quantum plasmon resonances of individual metallic nanoparticles, Nature 483 (7390) (2012) 421–U468.
[54] A. Roy, J. Ghose, Electrical and magnetic characterization of Rh_2O_3–I, Materials Research Bulletin 33 (4) (1998) 547–551.
[55] J. Coey, Acta Crystallographica Section B 26 (11) (1970) 1876–1877.